

Article

Leakage Current Conduction Mechanism of Au-Pt-Ti/HfO₂-Al₂O₃/n-InAlAs Metal-Oxide-Semiconductor Capacitor under Reverse-Biased Condition

He Guan and Shaoxi Wang * 

School of Microelectronics, Northwestern Polytechnical University (NPU), Xi'an 710072, China;

he.guan@nwpu.edu.cn

* Correspondence: shxwang@nwpu.edu.cn

Received: 29 August 2019; Accepted: 18 October 2019; Published: 1 November 2019



Abstract: Au-Pt-Ti/high-*k*/n-InAlAs metal-oxide-semiconductor (MOS) capacitors with HfO₂-Al₂O₃ laminated dielectric were fabricated. We found that a Schottky emission leakage mechanism dominates the low bias conditions and Fowler–Nordheim tunneling became the main leakage mechanism at high fields with reverse biased condition. The sample with HfO₂ (4 m)/Al₂O₃ (8 nm) laminated dielectric shows a high barrier height ϕ_B of 1.66 eV at 30 °C which was extracted from the Schottky emission mechanism, and this can be explained by fewer In–O and As–O states on the interface, as detected by the X-ray photoelectron spectroscopy test. These effects result in HfO₂ (4 m)/Al₂O₃ (8 nm)/n-InAlAs MOS-capacitors presenting a low leakage current density of below 1.8×10^{-7} A/cm² from –3 to 0 V at 30 °C. It is demonstrated that the HfO₂/Al₂O₃ laminated dielectric with a thicker Al₂O₃ film of 8 nm is an optimized design to be the high-*k* dielectric used in Au-Pt-Ti/HfO₂-Al₂O₃/InAlAs MOS capacitor applications.

Keywords: high-*k* dielectric; leakage current mechanism; interface characteristics

1. Introduction

According to the requirements of high speed, low power dissipation, and low noise application for RF devices used in telecommunication and other modern integrated circuits, increasing interest is focused on new III-V compound devices of InAs/AlSb and InAlAs/InGaAs HEMTs (high-electron mobility transistors), as these devices possess high electron mobility and peak velocity in the channel [1–5]. However, due to the narrow band gap of channels of these HEMTs, the devices suffer from serious current leakage which is considered as the biggest issue of InAs/AlSb and InAlAs/InGaAs HEMTs [6,7]. In this kind of device, InAlAs is most frequently used as the protective layer on the above barrier and as the gate contact semiconductor [1,3], and some reports proposed to deposit a high-*k* dielectric film on InAlAs, together with the gate electrode, to become a metal-oxide-semiconductor (MOS) capacitor isolated gate structure, in order to effectively suppress the leakage current. HfO₂ that presents a high dielectric constant is a popular candidate as the high-*k* dielectric [8–10], however it does not match well with InAlAs and the poor lattice match would degrade its performance [9]; Al₂O₃ is used frequently as the high-*k* dielectric as well [10,11], however its dielectric constant is not high enough, and that will lead to a lower EOT (effective oxide thickness) which is not beneficial for reducing device size. For improvement, the HfO₂-Al₂O₃ laminated dielectric layer is proposed, and in this new device structure, a compromised dielectric constant can be achieved and the leakage current can be effectively suppressed [12–14]. In our previous paper [13], the physical and electrical performance of the new Au-Pt-Ti/high-*k*/n-InAlAs MOS capacitors with HfO₂-Al₂O₃ laminated dielectric were studied in detail. However, its leakage current mechanism was not mentioned, and this scheme has been

covered in few other papers. To better understand the generation reason of the leakage current of the Au-Pt-Ti/HfO₂-Al₂O₃/n-InAlAs MOS capacitor, we study the leakage current mechanism of the new devices at different bias condition ranges in detail. As InAs/AlSb HEMTs and InAlAs/InGaAs HEMTs work under negative gate voltage bias conditions, we studied the reverse-bias leakage current mechanism in this paper as in the case of a real application.

2. Experiment

The device structure from bottom to top is a 350 μm semi-insulating InP substrate, a 200 nm InP buffer layer, a 500 nm Si-doped In_{0.5}Al_{0.5}As semiconductor layer with a doping concentration of $1 \times 10^{17} \text{ cm}^{-3}$ [15], a 12 nm oxide layer with Al₂O₃-HfO₂ dielectrics, and a metal with structure of Ti (20 nm)/Pt (20 nm)/Au (200 nm). The detailed schematic layer structures of the prepared sample can be found in our previous published paper [14]. In order to identify the impact of the thickness of the Al₂O₃ inserting layer, we manufactured two kinds of samples with an oxide layer of HfO₂ (4 nm)/Al₂O₃ (8 nm) laminated dielectrics (marked as Sample #1), and HfO₂ (8 nm)/Al₂O₃ (4 nm) laminated dielectrics (marked as Sample #2), respectively. The detailed fabrication process is listed in Table 1 [16–20].

Table 1. Process description of Au-Pt-Ti/HfO₂-Al₂O₃/n-InAlAs metal-oxide-semiconductor (MOS) capacitor.

Process Step	Process	Description
1	InP buffer layer deposition	MBE (molecular beam epitaxy) at 470 °C
2	InAlAs semiconductor layer deposition	MBE at 350 °C
3	Surface treatment of InAlAs	36–38% HCl solution for 1 min and a 7% (NH ₄)S solution for 15 min, then dry in N ₂
4	Al ₂ O ₃ film deposition	Pass precursor of Al element as TMA (trimethylaluminium) for 0.5 s, then pass N ₂ for 2 s in order to transfer the Al-base residue out, then pass precursor of O element as H ₂ O for 0.5 s. Repeat the above process steps to obtain the required thickness
5	HfO ₂ film deposition	Pass precursor of Hf element as TEMAH (tetrakis ethylmethylethylamino hafnium) for 1 s, then pass N ₂ for 2 s in order to drive off the Hf-base residue, then pass precursor of O element as H ₂ O for 1 s. Repeat the above process steps to obtain the required thickness
6	Post-deposition annealing (PDA)	Heat the film from ambient temperature to 380 °C in N ₂ over 15 s, annealing for 60 s, and then cool to ambient temperature over 300 s
7	Metal	Magnetron sputtering. Size of 150 μm × 150 μm

3. Measurement and Discussion

The leakage current measurement of the Au-Pt-Ti/HfO₂-Al₂O₃/InAlAs MOS-capacitors under reversed bias condition is shown in Figure 1. It is found that the leakage current density J achieves a significant low value below 10^{-6} A/cm^2 in the bias voltage V_g ranges from −3 to 0 V at a temperature of 30 °C for the both Sample #1 and #2. In particular, Sample #1 shows a much lower leakage current, below $1.8 \times 10^{-7} \text{ A/cm}^2$ from −3 to 0 V at 30 °C which is three times less than Sample #2 with the leakage current value below $6.5 \times 10^{-7} \text{ A/cm}^2$. This demonstrates that the thickness ratio of Al₂O₃ and HfO₂

films clearly impact the leakage current. We note that the electric field E of Al_2O_3 should be higher than that of HfO_2 , since the dielectric constant of HfO_2 is higher than that of Al_2O_3 . However, we simply formulate E by applying V/T_{ox} (T_{ox} is oxide thickness) in order to present an intuitive view of the leakage current changing trend. In addition, it is found that the leakage current density J increases as the temperature increases. This may be explained by the violent electron movements at high temperatures. To better understand the generation reason of the leakage current of the Au-Pt-Ti/ HfO_2 - Al_2O_3 /InAlAs MOS capacitor and the reason for the lower leakage current of the sample with the higher thickness ratio of Al_2O_3 and HfO_2 films, we will study the leakage current mechanism of the devices at different bias condition ranges and different temperatures in detail.

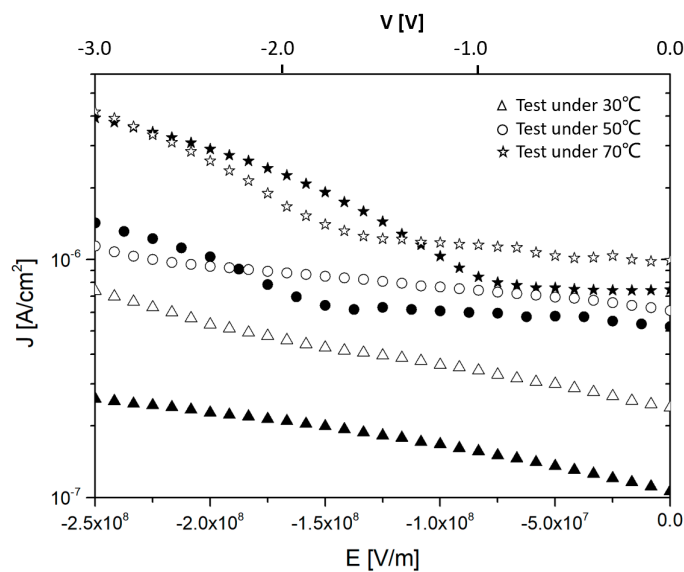


Figure 1. The leakage current measurement of the Au-Pt-Ti/ HfO_2 - Al_2O_3 /InAlAs MOS-capacitors under reversed bias condition at different temperatures. The solid symbol is for Sample #1 with HfO_2 (4 nm)/ Al_2O_3 (8 nm) laminated dielectrics, and the hollow symbol is for Sample #2 with HfO_2 (8 nm)/ Al_2O_3 (4 nm) laminated dielectrics.

Schottky emissions often happen in low electrical fields. The energy band diagram for Schottky emissions under the reversed bias condition is shown in Figure 2 [21–24]. Electrons surmount the metal– HfO_2 surface barrier first, and then surmount the barrier at HfO_2 - Al_2O_3 , and finally fall into the conduction band of InAlAs to form the leakage current. It can be verified by linear fitting the curve of $\ln J$ versus $E_i^{1/2}$ with a straight line, where J is the leakage current density and E_i is the electric field intensity under reversed bias voltage [25,26]. Schottky emission is temperature dependent, and the slope of linear approximation on the curve of $\ln J$ vs $E_i^{1/2}$ needs to be consistent at different temperatures, which is the typical feature of Schottky emission [11,25,26]. Therefore, we make the line fit on the measurement curve under different temperatures of 30/50/70 °C in order to identify it correctly by the same scope of the fitting straight line, as shown in Figure 3. According to the analysis, the Schottky emission occurs in the bias range of −1.1–0 V and −1.7–0 V for Sample #1 and Sample #2, respectively. As we presented before, Sample #1, with a higher thickness ratio of Al_2O_3 and HfO_2 films, shows a reduced leakage current in the Schottky region. This can be explained by its higher barrier height ϕ_B . The barrier height $\phi_{B,n}$ can be extracted from the equation $\phi_{B,n} = kT \ln(A^* T^2 / J_0) / q$ according to the Schottky emission mechanism, where k is the Boltzmann constant, T is the temperature, q is the electron charge, A^* is the effective Richardson constant as the value of $105600 \text{ A/K}^2 \text{ m}^2$, and J_0 is the saturation current density [15]. The extracted $\phi_{B,n}$ values are listed in Table 2. The $\phi_{B,n}$ we extracted was illustrated as in Figure 2. It presents the barrier at $\text{HfO}_2/\text{Al}_2\text{O}_3$ where is the top of the barrier. It is worth noting that the $\phi_{B,n}$ we obtained from the Schottky mechanism should be lower than the ideal barrier height by a value of $\Delta\phi_B$ as shown in Figure 2. This gap can be explained by the Schottky

barrier lowering effect [15,16]. It was found that Sample #1 presents a higher $\phi_{B,n}$ value than Sample #2, indicating that increasing the thickness of the Al_2O_3 film can suppress the accessibility of carriers to climb over the barrier to form a leakage current in the case of a fixed total thickness of laminated dielectric. In addition, it is noted that ϕ_B increases as the temperature is increased, while the leakage current is also increased as the temperature is increased (Shown in Figure 1). This is because electrons move more violently at high temperatures, making it easier for the electrons to cross through the even higher barrier between the oxide layer and the gate electrode, to form an increased gate leakage current. As a result, the samples show a clear, increased leakage current by one order of magnitude when the temperature was increased from 30 °C to 70 °C.

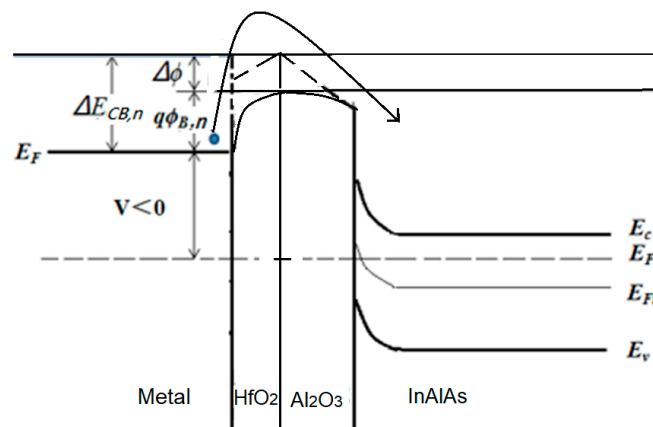


Figure 2. Schottky emission energy-band diagram for $V_g < 0$.

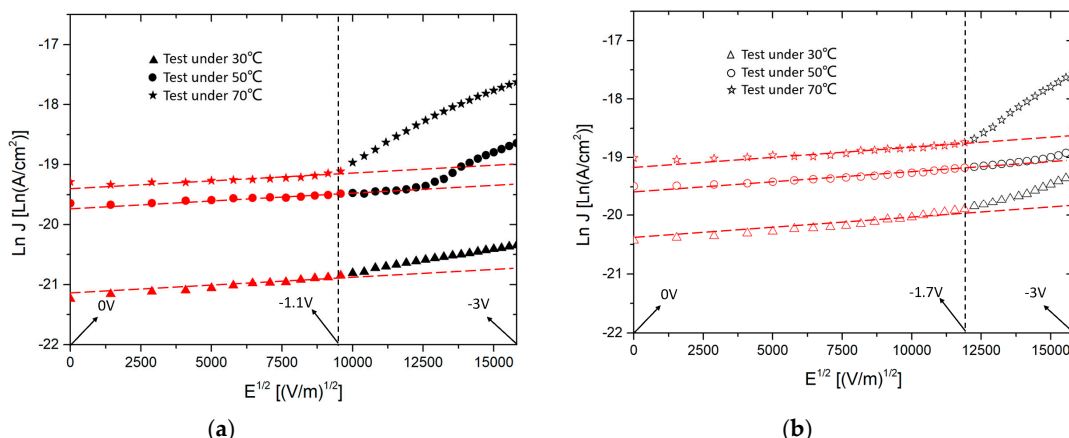


Figure 3. Schottky emission plots for MOS-capacitors at different temperatures. (a) Sample #1 with HfO_2 (4 nm)/ Al_2O_3 (8 nm) laminated dielectrics, (b) Sample #2 with HfO_2 (8 nm)/ Al_2O_3 (4 nm) laminated dielectrics.

Table 2. Extracted barrier height $\phi_{B,n}$ from the Schottky emission leakage mechanism at different temperatures.

	Sample #1 HfO_2 (4 nm)/ Al_2O_3 (8 nm)	Sample #2 HfO_2 (8 nm)/ Al_2O_3 (4 nm)
30 °C	1.66 eV	1.62 eV
50 °C	1.73 eV	1.70 eV
70 °C	1.83 eV	1.80 eV

As Schottky emission is strongly related to dielectric-semiconductor interfacial conditions, a 60 s etching process was applied to the dielectric surface in order to make the interface suitable for X-ray

photoelectron spectroscopy (XPS). An Al sputtering ion beam was applied in the XPS setup with a beam current density of 1.067×10^{-5} A/cm² under 12,000 V. The XPS spectra were calibrated against the C–C peak at 284.8 eV. Advantage software was used to analyze the XPS data, the binding energy peak positions indicate the chemical environment of the elements and the peak areas show the elemental composition. The measurements of the O 1s peak are shown in Figure 4. Figure 4a presents the XPS measurement of the O 1s peak of the dielectric-semiconductor interface, and Figure 4b presents the comparison of the ratio of various oxide contents on the interface. It is found that a larger amount of Al₂O₃ with O 1s peak at 532.25 eV is presented in Sample #1, compared with Sample #2, which leads to enhanced matching between the dielectric and semiconductor and benefits the interfacial quality. Sample #2 presents Al–O and In–O on the interface, which forms interface states to degrade the interface quality. In addition, Sample #2 shows higher HfAlO components on the interface as well. The HfAl–O chemical bond is not as stable as the Al–O chemical bond because of its lower affinity with the oxide atom, make it easy to generate oxygen vacancies and dangling bonds in the presence of impurities from the epitaxial process to form interface states, i.e., As–O and In–O states, leading to a higher concentration of interfacial states. Thus, the leakage current that was contributed by interfacial traps is higher for Sample #2 with thinner Al₂O₃ at 4 nm. Therefore, increasing the ratio of Al₂O₃ to HfO₂ is helpful to increase the interface quality, and to suppress the Schottky leakage current.

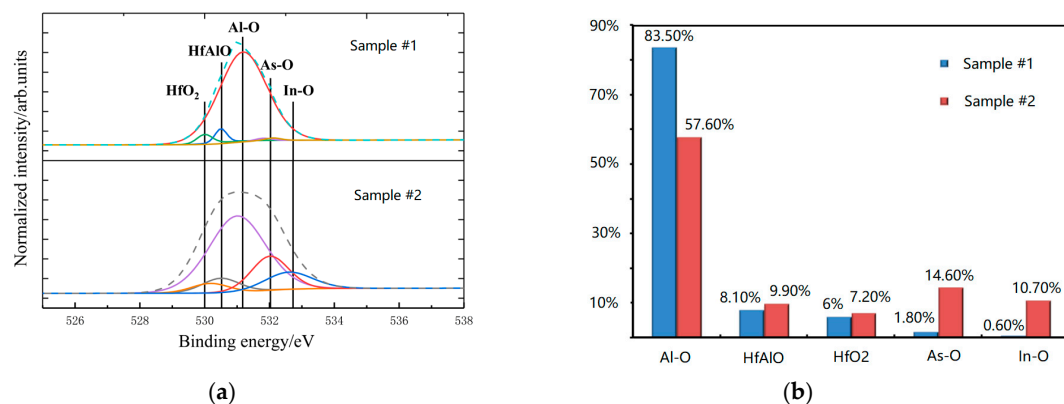


Figure 4. (a) X-ray photoelectron spectroscopy (XPS) measurement of the O_{1s} peak of the dielectric-semiconductor interface, (b) comparison of the ratio of various oxide contents on the interface.

When V_g is continually biased to the negative direction, the Fowler–Nordheim (F–N) tunneling, which can be verified by fitting the curves of $\ln(J/E_i^2)$ versus $1/E_i$ with a straight line [27–31], becomes the main leakage mechanism. According to the extraction in Figure 5, the F–N emission occurs in the range -3 – -1.1 V and -3 – -1.7 V, for Sample #1 and Sample #2, respectively. It indicates that when the electrical field intensity is large enough, the electrons obtain enough energy to tunnel the potential barrier to make F–N tunneling occur. It is noted that the slope of the F–N fitting straight line under different temperatures is not the same. This is because the F–N tunneling is not proportional to temperature [32], which is different from the Schottky emission mechanism. The effective barrier height can be extracted from the F–N fitting curve, and values are shown in Table 3. It is found that the barrier extracted for Sample #1 is higher than that of Sample #2 at 30 °C and 70 °C, resulting in Sample #1 showing a reduced leakage current in the F–N region at room temperature. In contrast, Sample #1 shows a lower barrier height, of 0.18 eV, than Sample #2, showing a barrier height of 0.26 eV with the temperature of 50 °C. This should make Sample #1 present a higher leakage current under the F–N region, which is consistent with the leakage current test result in Figure 1.

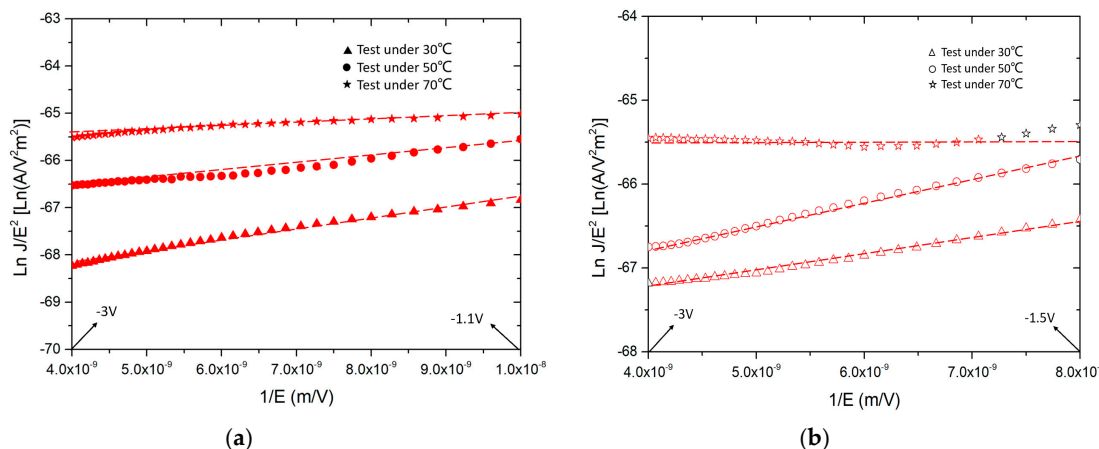


Figure 5. Fowler–Nordheim (F–N) tunneling plots for the MOS-capacitors. (a) Sample #1 with HfO_2 (4 nm)/ Al_2O_3 (8 nm) laminated dielectrics, (b) Sample #2 with HfO_2 (8 nm)/ Al_2O_3 (4 nm) laminated dielectrics.

Table 3. Extracted barrier height from the F–N leakage mechanism.

	Sample #1 HfO_2 (4 nm)/ Al_2O_3 (8 nm)	Sample #2 HfO_2 (8 nm)/ Al_2O_3 (4 nm)
30 °C	0.24 eV	0.21 eV
50 °C	0.18 eV	0.26 eV
70 °C	0.09 eV	0.03 eV

4. Discussion

The leakage current conduction mechanism of an Au-Pt-Ti/ HfO_2 - Al_2O_3 /InAlAs MOS-capacitor is dependent on the bias voltage. The Schottky emission occurs at a very low negative bias, and F–N tunneling becomes a dominant conduction mechanism when the electrical field intensity is increased continually. Due to the larger barrier height and lower interface states, the sample with HfO_2 (4 nm)/ Al_2O_3 (8 nm) laminated dielectric shows a very low leakage current density of below $1.8 \times 10^{-7} \text{ A/cm}^2$ from -3 to 0 V at 30°C . In conclusion, the HfO_2 (4 nm)/ Al_2O_3 (8 nm) laminated dielectric structure is an optimized design to be the high-k dielectric used in Au-Pt-Ti/ HfO_2 - Al_2O_3 /InAlAs MOS capacitors to suppress the leakage current.

Author Contributions: Software, formal analysis, investigation, writing—original draft preparation, H.G.; writing—review and editing, supervision, project administration, S.W.

Funding: This project was supported by National science foundation of Shaanxi province, China (Grant No. 2018JQ6069), China Postdoctoral Science Foundation, (Grant No. 2018M643733), The key research and development program of shaanxi province (Grant No. 2018GY-006).

Conflicts of Interest: The authors declare no conflict of interest.

References

- Moschetti, G.; Wadeffalk, N.; Nilsson, P.A.; Roelens, Y.; Noudeviwa, A.; Desplanque, L.; Wallart, X.; Danneville, F.; Dambrine, G.; Bollaert, S.; et al. InAs/AlSb HEMTs for cryogenic LNAs at ultra-low power dissipation. *Solid-State Electron.* **2011**, *64*, 47–53. [[CrossRef](#)]
- Moschetti, G.; Nilsson, P.; Wadeffalk, N.; Malmkvist, M.; Lefebvre, E.; Grahn, J. DC characteristics of InAs/AlSb HEMTs at cryogenic temperatures. In Proceedings of the Indium Phosphide & Related Materials (IPRM) International Conference, Newport Beach, CA, USA, 10–14 May 2009; p. 323.
- Malmkvist, M.; Lefebvre, E.; Borg, M.; Desplanque, L.; Wallart, X.; Dambrine, G.; Bollaert, S.; Grahn, J. Electrical characterization and small-signal modeling of InAs/AlSb HEMTs for low-noise and high-frequency applications. *IEEE Trans. Microw. Theory Tech.* **2008**, *56*, 2685–2691. [[CrossRef](#)]

4. Moschetti, G.; Wadeffalk, N.; Nilsson, P.A.; Abbasi, M.; Desplanque, L.; Wallart, X.; Grahn, J. Cryogenic InAs/AlSb HEMT wideband low-noise IF amplifier for ultra-low-power applications. *IEEE Microw. Wirel. Compon. Lett.* **2012**, *22*, 144–146. [[CrossRef](#)]
5. Malmkvist, M.; Lefebvre, E.; Borg, M. Characterization of insulated-gate versus schottky-gate InAs/AlSb HEMTs. In Proceedings of the European Microwave Integrated Circuit Conference, Munich, Germany, 8–10 October 2007.
6. Hashizume, T.; Ootomo, S.; Inagaki, T.; Hasegawa, H. Surface passivation of GaN and GaN/AlGaN heterostructures by dielectric films and its application to insulated-gate heterostructure transistors. *J. Vac. Sci. Technol. B* **2003**, *21*, 1828. [[CrossRef](#)]
7. Hashizume, T.; Anantathanasarn, S.; Negoro, N.; Sano, E.; Hasegawa, H.; Kumakura, K.; Makimoto, T. Al₂O₃ insulated-gate structure for AlGaN/GaN heterostructure field effect transistors having thin AlGaN barrier layers. *Jpn. J. Appl. Phys.* **2004**, *43*, 777. [[CrossRef](#)]
8. Trinh, H.D.; Lin, Y.C.; Wang, H.C.; Chang, C.H.; Kakushima, K.; Iwai, H. Effect of Postdeposition Annealing Temperatures on Electrical Characteristics of Molecular-Beam-Deposited HfO₂ on n-InAs/InGaAs Metal–Oxide–Semiconductor Capacitors. *Appl. Phys. Express* **2012**, *5*, 1104. [[CrossRef](#)]
9. Brennan, B.; Galatage, R.V.; Thomas, K.; Pelucchi, E.; Hurley, P.K.; Kim, J.; Hinkle, C.L.; Vogel, E.M.; Wallace, R.M. Chemical and electrical characterization of the HfO₂/InAlAs interface. *J. Appl. Phys.* **2013**, *114*, 104103. [[CrossRef](#)]
10. Liu, C.; Zhang, Y.M.; Zhang, Y.M.; Lv, H.L. Interfacial characteristics of Al/Al₂O₃/ZnO/n-GaAs MOS capacitor. *Chin. Phys. B* **2013**, *22*, 076701. [[CrossRef](#)]
11. Jin, C.J.; Lv, H.L.; Zhang, Y.M.; Guan, H.; Li, Z.; Zhang, Y. Study on reverse-biased gate leakage current mechanisms in Al₂O₃/InAlAs metal-oxide-semiconductor structures. *Thin Solid Films* **2016**, *619*, 48–52. [[CrossRef](#)]
12. Jin, C.J.; Lv, H.L.; Zhang, Y.M.; Guan, H.; Wu, L.; Lu, B.; Liu, C. Transport mechanisms of leakage current in Al₂O₃/InAlAs MOS capacitors. *Solid-State Electron.* **2016**, *123*, 106–110. [[CrossRef](#)]
13. Wu, L.; Zhang, Y.; Lv, H.; Zhang, Y. Interfacial and electrical characterization of HfO₂/Al₂O₃/InAlAs structures. *Jpn. J. Appl. Phys.* **2015**, *54*, 110303. [[CrossRef](#)]
14. Guan, H.; Jing, C.Y. Study on the Physical and Leakage Current Characteristics of an Optimized High-k/InAlAs MOS Capacitor with a HfO₂–Al₂O₃ Laminated Dielectric. *Coatings* **2018**, *8*, 417. [[CrossRef](#)]
15. Guan, H.; Lv, H. Study on leakage current mechanism and band offset of high-k/n-InAlAs metal-oxide-semiconductor capacitors with HfO₂ and HfAlO dielectric. *Thin Solid Films* **2018**, *661*, 137–142. [[CrossRef](#)]
16. Lin, Y.C.; Hai, D.T.; Chuang, T.W.; Iwai, H.; Kakushima, K.; Ahmet, P.; Lin, C.H.; Diaz, C.H.; Chang, H.C.; Jiang, S.M.; et al. Electrical Characterization and Materials Stability Analysis of La₂O₃/HfO₂ Composite Oxides on n-In_{0.53}Ga_{0.47}AsMOS Capacitors With Different Annealing Temperatures. *IEEE Electron Device Lett.* **2013**, *34*, 1229. [[CrossRef](#)]
17. Galatage, R.V.; Dong, H.; Zhernokletov, D.M.; Brennan, B.; Hinkle, C.L.; Wallace, R.M.; Vogel, E.M. Effect of post deposition anneal on the characteristics of HfO₂/InP metal-oxide-semiconductor capacitor. *Appl. Phys. Lett.* **2011**, *99*, 172901. [[CrossRef](#)]
18. Park, J.; Cho, M.; Kim, S.K.; Park, T.J.; Lee, S.W.; Hong, S.H.; Hwang, C.S. Influence of the oxygen concentration of atomic-layer-deposited HfO₂ films on the dielectric property and interface trap density. *Appl. Phys. Lett.* **2005**, *86*, 112907. [[CrossRef](#)]
19. Galatage, R.V.; Dong, H.; Zhernokletov, D.M. Electrical and chemical characteristics of Al₂O₃/InP metal-oxide-semiconductor capacitors. *Appl. Phys. Lett.* **2013**, *102*, 122109. [[CrossRef](#)]
20. Wheeler, D.C. High-k-InAs metal-oxide-semiconductor capacitors formed by atomic-layer deposition. Ph.D. Thesis, University of Notre Dame, Notre Dame, IN, USA, April 2009.
21. Huang, M.L.; Chang, Y.C.; Chang, Y.H.; Lin, T.D.; Kwo, J.; Hong, M. Energy-band parameters of atomic layer deposited Al₂O₃ and HfO₂ on In_xGa_{1-x}As. *Appl. Phys. Lett.* **2009**, *94*, 052106. [[CrossRef](#)]
22. Suri, R.; Kirkpatrick, C.J.; Lichtenwalner, D.J.; Misra, V. Energy-band alignment of Al₂O₃ and HfAlO gate dielectrics deposited by atomic layer deposition on 4H-SiC. *Appl. Phys. Lett.* **2010**, *96*, 042903. [[CrossRef](#)]
23. Yu, H.Y.; Wu, N.; Li, M.F.; Zhu, C.; Cho, B.J. Thermal stability of (HfO₂)_x(Al₂O₃)_{1-x}. *Appl. Phys. Lett.* **2002**, *81*, 3618–3620. [[CrossRef](#)]

24. Suzuki, R.; Taoka, N.; Yokoyama, M.; Lee, S.; Kim, S.H.; Hoshill, T.; Yasuda, T.; Jevasuwan, W.; Maeda, T.; Ichikawa, O.; et al. 1-nm-capacitance-equivalent-thickness $\text{HfO}_2/\text{Al}_2\text{O}_3/\text{InGaAs}$ metal-oxide-semiconductor structure with low interface trap density and low gate leakage current density. *Appl. Phys. Lett.* **2012**, *100*, 132906. [[CrossRef](#)]
25. Quah, H.J.; Cheong, K.Y. Current conduction mechanisms of RF-magnetron sputtered Y_2O_3 gate oxide on gallium nitride. *Curr. Appl. Phys.* **2013**, *13*, 1433–1439. [[CrossRef](#)]
26. Chiu, F.C. Electrical characterization and current transportation in metal / Dy_2O_3 / Si structure. *J. Appl. Phys.* **2007**, *102*, 044116. [[CrossRef](#)]
27. Cheong, K.Y.; Moon, J.H.; Kim, H.J.; Bahng, W.; Kim, N.K. Current conduction mechanisms in atomic-layer-deposited HfO_2 /nitride SiO_2 stacked gate on 4H silicon carbide. *J. Appl. Phys.* **2008**, *103*, 084113. [[CrossRef](#)]
28. Chanana, R.K.; McDonald, K.; Di Ventra, M.; Pantelides, S.T.; Feldman, L.C.; Chung, G.Y.; Tin, C.C.; Williams, J.R.; Weller, R.A. Fowler–Nordheim hole tunneling in p-SiC/ SiO_2 structures. *Appl. Phys. Lett.* **2000**, *77*, 2560–2562. [[CrossRef](#)]
29. Zhang, H.; Miller, E.J.; Yu, E.T. Analysis of leakage current mechanisms in Schottky contacts to GaN and $\text{Al}_{0.25}\text{Ga}_{0.75}\text{N}/\text{GaN}$ grown by molecular-beam epitaxy. *J. Appl. Phys.* **2006**, *99*, 023703. [[CrossRef](#)]
30. Fiorenza, P.; Greco, G.; Giannazzo, F.; Lo Nigro, R.; Roccaforte, F. Poole–Frenkel emission in epitaxial nickel oxide on AlGaN/GaN heterostructures. *Appl. Phys. Lett.* **2012**, *101*, 172901. [[CrossRef](#)]
31. Choi, Y.; Kang, S.; Cha, S.H.; Kim, H.S.; Song, K.; Lee, Y.J.; Kim, K.; Kim, Y.S.; Cho, S.; Park, Y. Platycodon saponins from Platycodi Radix (Platycodon grandiflorum) for the Green Synthesis of Gold and Silver Nanoparticles. *Nanoscale Res. Lett.* **2018**, *13*, 23. [[CrossRef](#)]
32. Agarwal, A.K.; Seshadri, S.; Rowland, L.B. Temperature dependence of Fowler–Nordheim current in 6H-and 4H-SiC MOS capacitors. *IEEE Electron Device Lett.* **1997**, *18*, 592–594. [[CrossRef](#)]



© 2019 by the authors. Licensee MDPI, Basel, Switzerland. This article is an open access article distributed under the terms and conditions of the Creative Commons Attribution (CC BY) license (<http://creativecommons.org/licenses/by/4.0/>).